C 4 Single-Molecule Mechanics and Force Spectroscopy

V. Walhorn[1], T. Dierks, J. Mattay[2], N. Sewald[2] and D. Anselmetti[1]

[1]Faculty of Physics, Bielefeld University, Universitätsstr. 25
33615 Bielefeld

[2]Faculty of Chemistry, Bielefeld University, Universitätsstr. 25
33615 Bielefeld

Contents

1 Introduction & Motivation

How do molecules interact with each other? When Emil Fischer proposed his key and lock model in 1894 he introduced a completely new perspective on the interplay of molecules [1]. Briefly, as he investigated the catalytic activity of invertase and β-amylase towards different polysaccharides he found that both enzymes exclusively digest distinct polysaccharides. With virtually no knowledge about the protein 3D-structure he attributed these findings to the complementary shape of the reaction partners. Today we know that due to recognition forces these host guest systems specifically bind to each other. These interactions are governed by multiple comparable weak (and unspecific) interactions like hydrogen bonds, van-der-Waals and electrostatic forces or donor-acceptor interactions between complementary surfaces. However, in collaboration all these minute contributions sum up to highly specific and comparably strong bonds. Consequently, the functionality of many (bio-) chemical systems is governed by molecular recognition. Typical examples are the specific interaction of antibody and antigen, receptor and ligand, complementary DNA strands or supramolecular compounds that (self-) assemble to structures of higher complexity.

The understanding of the impact how (weak) molecular forces act on and between (single) molecules, is highly relevant for understanding and controlling the macroscopic properties and processes (for instance the immune response, (cellular) adhesion phenomena or the structural integrity of materials). In the last decade, single molecule force spectroscopy techniques have contributed a wealth of information on the impact of forces on the molecular scale that go beyond the common knowledge of macroscopic force experiments and hitherto have not been accessible. Upon stretching individual (bio-) polymer strands [2] as well as investigating and quantifying the interaction forces between macromolecules [3-5] a deep insight into elapsed force and binding mechanisms, their associated reaction pathways and reaction kinetics could be investigated. Furthermore, many experimental and theoretical verifications allowed to establish a coherent framework where the stochastic, thermally driven reactions at the single molecule level could be related to the macroscopic properties (observables) or thermodynamic state variables of a molecular ensemble (ergodic principle).

Within this survey, we briefly introduce general experimental concepts and the theoretical framework of single molecule force spectroscopy spectroscopy which is mandatory to analyze the data in a quantitative manner. The latter is fundamentally described by the Kramers-Bell-Evans theory (KBE-theory), which provides a coherent bridge between the nanoscopic force values determined in single-molecule experiments and the macroscopic ensemble parameters of the analyzed system (e.g. dissociation rate constants). Furthermore, we give a brief summary of certain publications to give an overview of contemporary SMFS applications.

2 Single Molecule Mechanics – General Concepts

Single molecule force spectroscopy (SMFS) has proven to significantly contribute in molecular binding studies to quantitatively determine:

- forces required to disrupt inter- and intramolecular (non)covalent bonds
- molecular elasticities (as mentioned before)
- dissociation rate constants (average lifetime of the complex)

- dimerization equilibrium constants
- details of the binding energy landscape
- entropic and enthalpic forces and energies required to stretch single molecules
- binding properties of "insoluble" molecules in solvent environment

in and between surface-bound but "unlabelled" molecules in an affinity range of 10^{-4}-10^{-15} M at the sensitivity of single point mutations or structural variations.

Here, we focus on typical intermolecular bond strengths (recognition forces) that are within the range of 40-200 pN and can nicely be accessed and investigated with several single molecule force spectroscopy techniques like atomic force microscopy (AFM), magnetic and optical tweezers, micropipettes etc. The experimental concepts presented here concentrate on AFM based SMFS. However, they commonly can be adapted to other SMFS techniques with ease.

In SMFS, two molecular binding partners of interest have to be immobilized and covalently bound to opposing surfaces (i.e. cantilever tip and sample surface). In order to first let the molecules associate, both surfaces will be approached to each other and brought into contact. Upon withdrawing the surfaces, a molecular binding event can be detected when the force transducer (cantilever) is withheld at the opposing surface. Repeated approaching and withdrawing (also termed as force cycle) result in force distance curves (Fig. 2a). There, the force acting on the AFM tip is plotted against its vertical position (piezo extension), where a molecular dissociation event can be identified by a sudden jump in the "attractive" force regime back to the curve at zero force (F=0).

2.1 Receptor-Ligand Dissociation Kinetics

In thermal equilibrium non-covalently bound molecular complexes associate and dissociate at the same rate k_{on}^0 and k_{off}^0, respectively. This is easily expressed by the law of mass action

$$[L] + [R] \underset{k_{off}^0}{\overset{k_{on}^0}{\rightleftharpoons}} [LR],$$

where $[L]$ and $[R]$ are the concentrations of the ligand and receptor, and $[LR]$ denotes the concentration of the molecular complex. The complex dissociates thermally when it is driven across the activation energy barrier $\Delta G^{\#}$ (Fig 1). Correspondingly, the dissociation rate constant is expressed as follows:

$$k_{off}^0 = C\ exp\left(-\frac{\Delta G^{\#}}{k_B T}\right) \quad (1)$$

However, the pre-exponential factor C is commonly unknown and therefore k_{off}^0 cannot be estimated directly. The central concept in SMFS is to lower the activation energy $\Delta G^{\#}$ by applying an external force f and observe the force dependency of the molecular dissociation process. Correspondingly, the dissociation rate k_{off}(f) under external force can be expressed as

$$k_{off}(f) = C\ exp\left(-\frac{\Delta G^{\#} - f x_{\beta}}{k_B T}\right) \quad (2)$$

$$\Leftrightarrow k_{off}^{0}\ exp\left(\frac{f x_{\beta}}{k_B T}\right) \quad (3)$$

where x_β is the so-called interaction length (also termed as reaction length).

Generally, one can discriminate between two experimental techniques: In the force ramp approach the molecular complex is loaded at an arbitrary but constant velocity (f becomes a function of time) and the dissociation forces F_{diss} are acquired (Fig 2a). Typically, hundreds to thousands individual force curves have to be measured and combined in a force histogram (Fig. 2a inset). These show a certain scatter since the process of molecular dissociation is of stochastic nature. The most probable dissociation force F_{max} can be determined by fitting an appropriate distribution function (like a Gaussian) to the measured force histogram.

The first theoretical description has been first published by Evans and Ritchie [6] who applied the general picture of the Kramers-rate based Bell adhesion model to this nanobiological dissociation problem with a ramped external force [7, 8]. Since the velocity of the force transducer in this active force-induced dissociation process is relatively slow (compared to the Brownian motion of the molecules) it can be described as a thermally activated decay with a force-dependent activation energy.

Within this model the theory predicted an increase of the observed dissociation forces with increasing loading rate, as it could be verified in many single molecule experiments in the last decade.

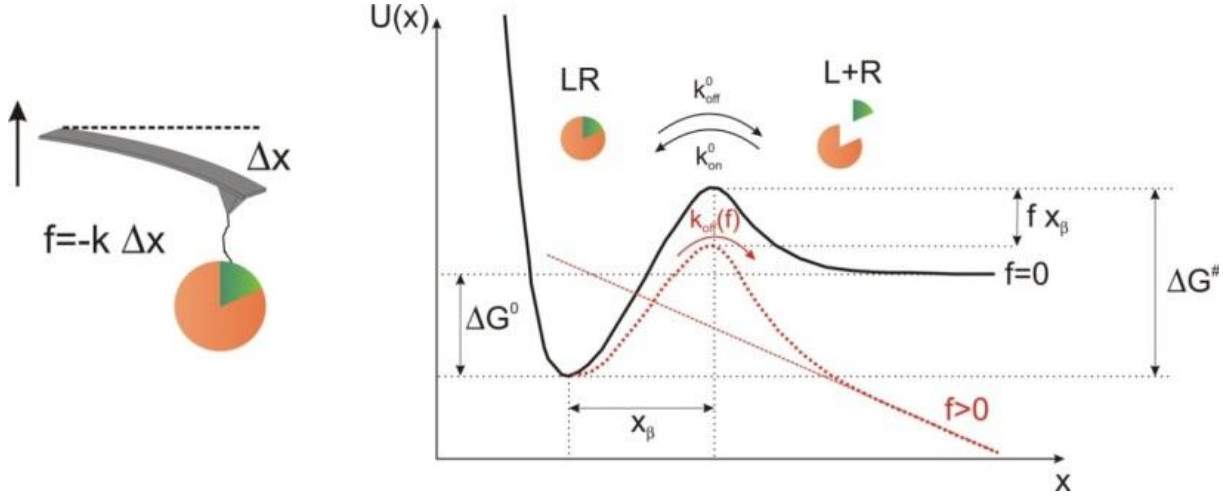

Fig. 1: *General concepts of SMFS. Left, a force f applied on a molecular complex can be estimated easily by the product of the cantilever spring constant k and the cantilever deflection* $\boldsymbol{\Delta x}$*. Right, molecular binding potential without (black) and with (dotted red) external force. By applying a force the activation energy barrier* $\boldsymbol{\Delta G^{\#}}$ *is lowered by* $\boldsymbol{f\ x_\beta}$*.*

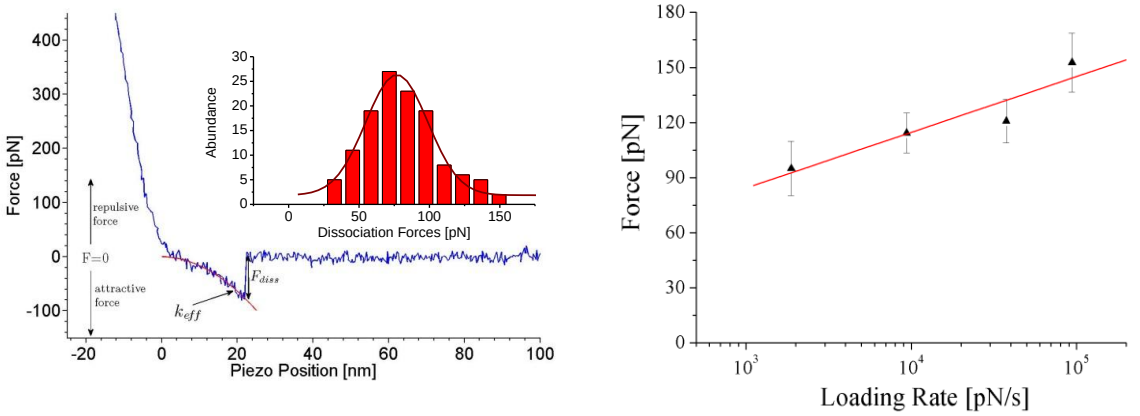

Fig. 2: *a) Typical force-distance curve (only retract curve) exposing a single molecule dissociation event. The dissociation Force F_{diss} is equal to the step height of the graph whereas the effective spring constant k_{eff} of the cantilever linker system is approximated by estimating the slope at the point of dissociation. The unbinding forces of several dissociation events are plotted in a histogram and the most probable dissociation force F_{max} can be estimated by approximation of a suitable distribution (inset). b) Semi-logarithmic scatter plot of F_{max} versus the loading rate (pulling velocity times effective spring constant). Equation 4 is approximated to the data to estimate $\boldsymbol{k_{off}^0}$ and $\boldsymbol{x_\beta}$(red plot).*

The most probable dissociation force F_{max} can be estimated with ease by:

$$F_{max} = \frac{k_B T}{x_\beta} \ln \frac{x_\beta \, r}{k_B \; T \; k_{off}^0} \tag{4}$$

F_{max} obviously depends logarithmically on the loading rate r which is the product of the experimental ramp speed v and the molecular elasticity k_{eff} (effective spring constant). The latter can be estimated as a linear fit to the force-distance curve just before dissociation (Fig.2a). The parameters x_β and k_{off} can now be extracted by fitting the experimental $F_{max} - r$ data in a semi-logarithmic representation (Fig.2b). Whereas the reaction coordinate x_β represents the distance between the minimum of the molecular binding potential and the transition state (activation energy) and can therefore be interpreted as the depth of the binding pocket (energy landscape, see Fig.1), the off-rate constant is defined as a kinetic parameter in thermal equilibrium of a molecular ensemble (mass action law). From a physical point of view, $k_{off}^{-1} = \tau$ is the average lifetime of the complex and gives information on the stability of the complex.

In force clamp SMFS a molecular complex is probed with a constant external force f until it dissociates (Fig.3a). Likewise, several single molecule dissociation events (individual life-times) have to be acquired. According to $N(t) = N_0 \; exp\left(-\frac{t}{\tau}\right)$ the average life-time τ for a given force is estimated by logarithmically plotting the number of intact bonds $N(t)$ versus time and approximating the (negative) linear slope to the dataset (Fig.3b). This procedure is repeated for several loading forces. The resulting dataset can be approximated by the inverse of equation 3 to estimate the complex life-time in thermal equilibrium τ ($k_{off}^{-1} = \tau$) and the reaction coordinate x_β (Fig.3c). Evidently, both approaches are equivalent as they both yield

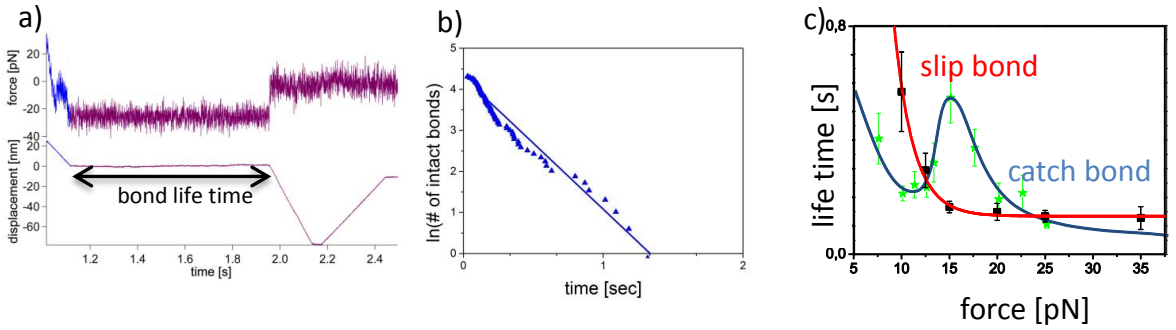

Fig. 3: *a) Force clamp dataset. The force acting on the cantilever and the piezo displacement are plotted versus time. The marked constant regime can be attributed to the life time of a molecular complex. b) N(t) plotted versus time for several individual life time measurements. The average complex life time is approximated by the slope of the plots. c) The average life times for several clamp forces (scatter plot) are approximated by equation 3 in the case of (common) slip bond dissociation (red graph) or by an appropriate catch bond model which will be introduced in chapter 1.3.4.*

the complex life time τ and the reaction coordinate x_β. However, dynamic force spectroscopy is much more common as the experiments can be conducted faster and the experimental setup does not need a precise and robust feedback loop for the load control.

Unfortunately, independent of the experimental approach the on-rate constant k_{on} cannot simultaneously be accessed, which makes a determination of the dissociation constant (constant of equilibrium) $K_d = k_{off}/k_{on}$ or the binding energy $E_b = k_BT \ln K_d$ difficult. However, in the limit of a diffusion-controlled reaction, an estimate of $k_{on} = k_{smol}$ via the Smoluchowski theory is possible, allowing for a quantitative approach to determine K_d and therefore an affinity ranking of the molecules involved [9]. Here, $k_{smol} = 4\pi R D_{SE} N_A$, where R, D_{SE}, N_A denote interaction distance, diffusion coefficient (Stokes-Einstein: $D_{SE} = k_BT/6 \pi \eta r_{prot}$) and Avogadro number, respectively.

2.2 Receptor-Ligand Interactions at the Single Molecule Level

2.2.1 Biomolecular Receptor-Ligand Interaction

Molecular recognition between receptors and their related ligands govern countless processes in biological systems such as immune response, enzymatic activity, signal transduction or genome replication. Despite the detailed knowledge about the structure and function of the corresponding receptor-ligand complexes, information about their association and dissociation kinetics is often lacking. Apart from ensemble techniques like surface plasmon resonance (SPR) or isothermal titration calorimetry (ITC) SMFS can be a powerful means to explore host guest interactions especially when the availability of the compounds is limited due to low yield synthesis/expression or if the binding partners expose a low affinity (dissociation constant K_D in the micromolar range).

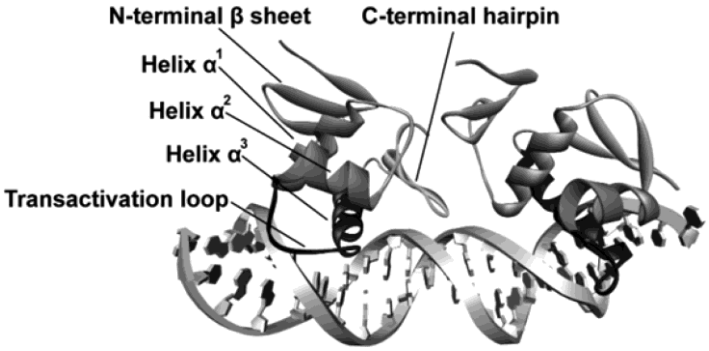

Fig. 4: *Crystal structure of two PhoB^{DBD}-proteins bound to a pho box in a head-to-tail arrangement. Figures adapted with courtesy [10].*

The transcription factor PhoB is a protein that is part of a two-component signal transduction system. Briefly, the transmembrane protein PhoR activates PhoB by phosphorylation of Asp53 in the regulatory domain and the concomitant structural change enables PhoB to bind to its cognate Pho boxes in the promoter region [10, 11]. This causes an alteration of DNA structure in the complex that enables interaction of the RNA polymerase with PhoB and subsequently with DNA, thus activating the transcription and biosynthesis of proteins. Notable, at least 287 genes are differentially expressed in the presence of active PhoB.

Here, the recognition and binding is a cooperative process, that is mediated multiple structural features. The DNA binding domain (DBD) of PhoB comprises a so-called winged helix-turn-helix recognition (wHTH) motif. An alpha helical recognition helix (α^3) mainly interacts with the major groove of the cognate DNA, a second helix (α^2) stabilizes the protein DNA complex, and a c-terminal beta hairpin penetrates the minor groove of the DNA recognition sequence (Fig.4). In order to analyze the recognition and to elucidate the minimal requirement for this cooperative binding process Wollschläger et al. analyzed the affinity of the whole DBD of PhoB (comprising the complete wHTH) and the α^3-recognition helix alone towards the cognate DNA sequence, respectively (Fig.4). Furthermore they introduced point mutations at selected loci in the α^3-recognition helix and observed the impact on the binding properties. The DNA–protein complex dissociates with k_{off}=0.0025 s^{-1}, which corresponds to an average life time of t=400 s. In comparison, the results obtained with the wild-type the α^3recognition helix alone yielded k_{off}= 3.1s^{-1}, thus indicating that the protein complex with the entire DBD

		k_{off} [s^{-1}] peptide (A) PhoB (190-209)	τ [s]		k_{off} [s^{-1}] protein (B) PhoB (127-229)	τ [s]
◆ wildtype	(1)	3.1 ± 2.1	0.32	(5)	0.0025 ± 0.0021	400
■ R193A	(2)	0.071 ± 0.053	14	(6)	0.012 ± 0.008	83
▲ H198A	(3)	50 ± 21	0.020	(7)	0.76 ± 0.25	1.3
R203A	(4)	—	—	(8)	—	—

Fig. 5: *AFM–DFS of PhoB peptides and proteins. A) PhoB peptides 190–209. B) PhoB DBD 127–229. k_{off}: dissociation rate constant for the peptide/protein DNA complexes; $\boldsymbol{\tau = {}^{1}/_{k_{off}}}$: complex lifetime. The kinetic data were measured in 100mM Na2HPO4/50mM NaCl (pH 7.4). Figure adapted with courtesy from [11].*

dissociates about 1000 times more slowly, most likely because the full DBD incorporates additional amino acid residues that support complex stabilization.

Things are different when comparing the lifetimes of the mutants R193A and H198A on the protein and peptide level (R203A exhibited no binding). In both mutants the full protein sequences, i.e. the DNA binding domain PhoB (127-229), yield a distinctly longer lifetime than the mutated PhoB(190–209) peptide sequences. For protein mutant R193A (6) the lifetime is 83s, and the result for peptide mutant R193A (2) is 14 s (Fig.5). As shown by the work of Wollschläger et al., SMFS can reveal subtle differences between single point mutants that could not be detected to this extent with other methods. The results are of special interest for the future design of synthetic peptide and protein ligands as artificial DNA binders and transcription factors in synthetic biology.

2.2.2 Supramolecular Host-Guest Systems: Calixarenes

Supramolecular chemistry, which has been defined as "*the chemistry beyond the molecule*" [12, 13] deals with the chemistry and collective behavior of organized ensembles of molecules [14] where the rational and synthetic fabrication of molecular structures of increasing size, complexity and functionality is possible. Within this concept calix [4] arenes are versatile building blocks in supramolecular chemistry because of their three-dimensional structure and the various functionalizations that can be introduced at different positions of the molecular framework. Their ability to adopt chalice-like conformation makes them ideally suited as the basis for molecular receptors (Fig.6a,b).

Furthermore, well-defined self-assembled monolayers on gold can also be obtained if thioether moieties are introduced at the part termed the "lower rim" of the molecule.

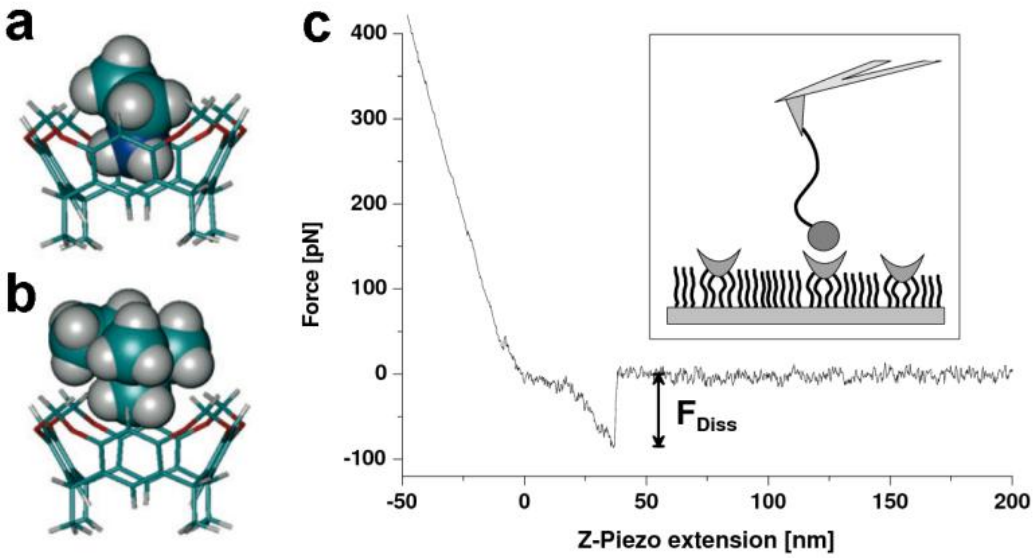

Fig. 6: *Supramolecular host-guest complex structure with calixarene cavitand and (a) an ethyl ammonium ion and (b) an ethyl trimethyl ammonium ion. (c) Typical single molecule force-distance curve of complex a) exhibiting an unbinding or dissociation force of ~85 pN. Inset: experimental scheme. Figures adapted with courtesy from [25a].*

In 2005 at Bielefeld University, the first single molecule study of supramolecular complex formation in a calixarene system was published, where the data could be quantitatively analyzed in accordance with the theoretical KBE standard model – a result that was in contrast to the one described above. Here, ammonium derivatives as the guest ligands were measured against resorcin[4]arenes cavitands in ethanol at room temperature using commercial instrument that was equipped with custom-made control and data acquisition system [15,16] [25a,d]. The 2,8,14,20-tetra-(10-(decylthio)decyl) cavitands were immobilized in diluted cavitand monolayers in a 1:40 mixture with didecylsulfide. The guest cations (ammonium (**A**), trimethyl ammonium (**TMA**) and triethyl ammonium (**TEA**), carrying one chemically modified entity each) were covalently attached to the AFM tip via a flexible polyethylene glycol (**PEG**) linker.

In AFM-SMFS experiments molecular dissociation events could be identified (Fig.6c) whereas their specificity could be verified in competition experiments (Fig.7a).
Interestingly, only the two smallest guests **A** and **TMA** were able to specifically bind to the cavitand, whereas the large **TEA** cation with a calculated diameter of 0.8 nm was sterically not able to enter the 0.7 nm wide host cavity.

Loading rate dependent dynamic force spectroscopy experiments and quantitative binding analysis according to the KBE-theory yielded k_{off} = (0.99 ± 0.81) s^{-1} for **A** and k_{off} = (1.87 ± 0.75)×10^{-2} s^{-1} for the **TMA** residue, resulting in a bond lifetime of τ = 1.01 s and τ = 53.5 s, respectively. This finding, together with the results of the competition experiments, indicates that the **TMA** residue fits tighter into the receptor cavity, ensuring a rise in binding affinity as compared to **A**.

Upon assuming a diffusion limited association with a typical on-rate constant of k_{on} = 10^5 $M^{-1}s^{-1}$, equilibrium constants for these reactions of K_{diss} = 0.99 $s^{-1}/10^5$ M^1s^{-1} = 10^{-5} M (corresponding to ΔG = -28 kJ mol^{-1}) and of K_{diss} = 2×10^{-2} $s^{-1}/10^5$ $M^{-1}s^{-1}$ = 2×10^{-7} M (corresponding to ΔG = -38 kJ mol^{-1}) for **A** and **TMA** ions, respectively, can be deduced. From the inverse slope of the loading rate dependency (Fig.7b) the molecular reaction length can be extracted yielding x_β = (0.22 ± 0.04) nm for **A**, and x_β = (0.38 ± 0.06) nm for the **TMA** ions. These estimated values qualitatively scale with calculated van-der-Waals diameters of 0.3 nm for **A** and 0.6 nm for **TMA**, respectively.

Therefore we can conclude that hydrogen bonds (not present in the **TMA** cavitand interaction) and cation-π-interactions have to contribute considerably to the molecular binding mechanism. Especially, the **TMA** cavitand system may profit from the latter contribution due to its positive charge distribution, which is shown to reside on the hydrogen atoms of the methyl groups.

2.2.3 Host-Guest Systems: Photoswitchable Calixarene Systems

The introduction of additional functionality and external control to mesoscopic systems is fascinating by itself, however, also aims for the rational design and directed synthesis of supramolecules that can mimic the function of biomolecules in distinct biomedical and technical applications. With this reverse engineering approach artificial and robust molecular motors and synthetic machines can be anticipated. Since future nanomachines rely on cyclic operation and external control, repetitive transition between at least two different molecular states e.g. by the conformational transition (switching) between two structural isomers is mandatory. As external control mechanism and transition stimulus the interaction of

a) b)

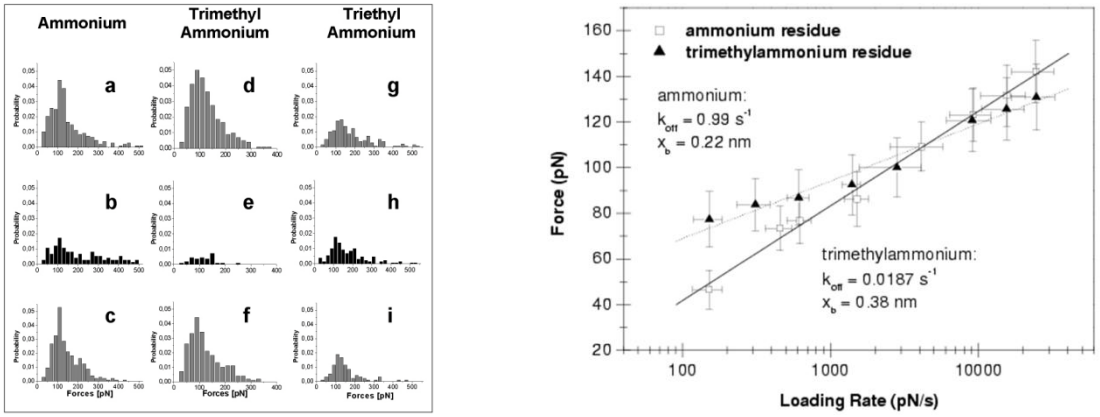

Fig. 7: *a) Activity status of probed cavitand surfaces against the three different ligands. (a,d,g) Single molecule force histograms measured in ethanol; (b,e,h) Control experiment: Single molecule force histograms in ethanol saturated with free competitive ions; (c,f) Reactivating the surface: single molecule force histograms after washing with pure ethanol restored the original unbindig probability. (Whereas the ammonium and trimethyl ammonium ligands exhibited specific interaction, only unspecific binding could be verified with the triethylammonium ligand (g,h,i)). b) Dynamic force spectroscopy. The loading rate dependent dissociation forces are logarithmically plotted for the binding of the ammonium and trimethyl ammonium guest residues to the resorc[4]arene cavitand. Figure adapted with courtesy from [16].*

molecules with light, electric, chemical or mechanical potentials are known. External activation via electronic excitation, energy transfer, and/or ionic transport by light harvesting complexes or energy up conversion in photosynthesis is well known.

Fundamental for all these processes is the ability to convert electromagnetic energy into conformational changes where specific and noncovalent bonds can be formed and released due to affinity changes. In order to investigate such phenomena in an artificial model system, we have synthesized a bistable supramolecular host-guest system where the supramolecular receptor cavity of the aforementioned resorcin [4] arene cavitand has been combined with two photodimerizable anthracene moieties whose structures can externally switched by UV-light and temperature [15, 17, 18].

Since the photodimerization process blocks the entrance of the cavitand, the affinity properties of this photochemical macrocycle was investigated in AFM-SMFS experiments against guest cation complexation. (For scheme see Fig.8a). The transition from the open (active) to the closed (inactive) structure of this photochemical single-molecule switch and vice versa was performed by irradiation with a UV lamp at (368 ± 7) nm for 5 min and locally heating the sample to 60°C for 2 h, respectively.

Whereas the macroscopic switching properties were analyzed and verified in UV absorption experiments (see Fig.8b) the nanoscopic affinity modulation of this optical switch was investigated by AFM-SMFS, where the photoactive cavitand was immobilized on a gold

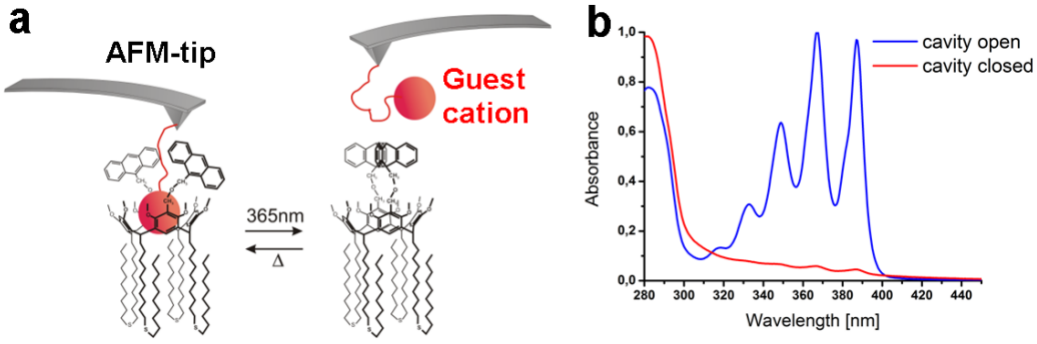

Fig. 8: *Resorcin[4]arene photoswitch. (a) Pictogram visualizing the photoactive cavitand receptor that is affinity probed against its ammonium cation ligand by AFM-SMFS. The switching between the open (active) and closed (inactive) structure is externally controlled by UV-light and thermal energy and mimics biological regulation triggers. (b) Resorc[4]arene photoswitch UV absorption spectrum for the open and closed isomer. The observed peaks for the open isomer are characteristic for the anthryl groups. Figures adapted with courtesy from [18].*

surface in a SAM in a 1:40 dilution with di-n-decyl sulfide. The guest molecule, an ammonium ion, was immobilized via a PEG-linker to the AFM tip.

Five series of AFM-SMFS experiments were performed in ethanol and presented as force histograms in Fig.9. As we have seen before, force histograms can be used as activity monitor. Fig.9a-d summarize the consecutive single molecule activity of the photoactive cavitand against ammonium complexation during the following stages: (a) open isomer after heating, (b) closed configuration after UV exposure, (c) (re)opened isomer after heating, (d) open isomer blocked with free ammonium and (e – image not shown) open isomer with full activity after washing with ethanol. These experiments prove that the photoactive resorc[4]arene cavitand can be reversibly switched between two different isomers that can be affinity probed by AFM-SMFS. Whereas one of the two isomers shows a high affinity to ammonium, the other exhibits almost none. Interestingly, the transition between the two isomers and its change in complexation affinity is of course related to a change in 3D structure of this supramolecular macrocycle.

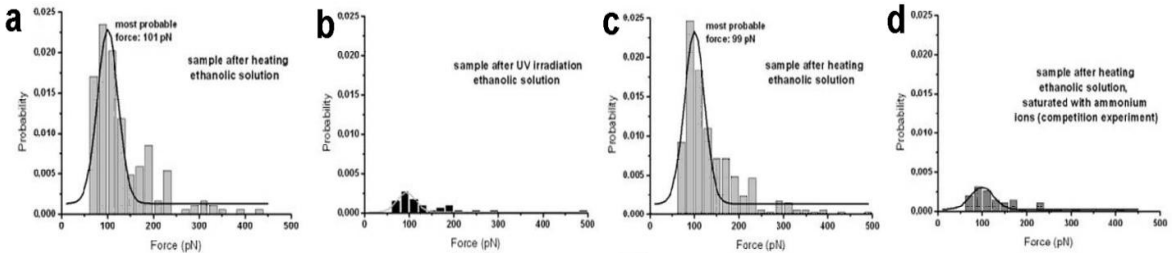

Fig. 9: *Single molecule force histograms of the resorcin[4]arene photoswitch. (a) Experimental series after heating the sample to 60°C for 2 h (open isomer and active state). (b) Series after irradiating the sample at 368 nm for 5 min (closed - inactive). (c) Series after renewed heating the sample for 2 h (open - active). (d) Series of competition experiments, performed in ethanol solution saturated with free ammonium (open/blocked - inactive). All experiments were performed with the same AFM tip and cavitand surface at a retract velocity of 1000 nm s^{-1}. Figures with courtesy from [18].*

2.2.4 Counter Intuitive Receptor-Ligand Interaction - Catch Bonds

As denoted before, noncovalent biological adhesion involves a multitude of different aspects like binding affinities, selectivities, multidomain interaction, force and/or allosteric regulation and many different molecular materials. Biophysically, we distinguish between slip and catch bonds. Whereas slip bonds are weakened, catch bonds are strengthened by tensile mechanical forces, respectively. Slip bonds were originally introduced by Bell in 1978 and mathematically treated within the framework of chemical reaction rate theory [7]. Catch bonds were conceptually introduced in 1988 by Dembo and co-workers [19]. Their experimental proves are tightly connected to the biological leukocyte recruitment system P-selectin (PSel) and its P-selectin glycoprotein ligand 1 (PSGL-1) [20]. Although, in the meantime numerous examples of slip bond-like interactions [4, 11, 15, 16, 21-29] could be demonstrated only a handful of catch bond systems could be identified in cellular and molecular force assays [30-34].

As mentioned in the Concepts section force ramp and force clamp SMFS yield the same bond parameters. However catch bonds are most commonly explored by the latter as the prolonged life time can be directly discerned from the resulting force-life time plot.

Beyond its experimental findings a couple of theoretical models were formulated helping to rationalize this counter-intuitive phenomenon. Here, we will briefly sketch two common models: The first approach was to introduce an alternative dissociation pathway along which the system can dissociate against low external forces resulting in a tightening of the bond [35-37]. At a certain critical force the system reaches its maximum stability and switches to the slip dissociation path. This approach is commonly referred to as one state two path model. The dependence of the dissociation rate k(f) on the applied force is given by

$$k(f) = k_c \exp\left(\frac{f\,x_c}{k_B T}\right) + k_s \exp\left(\frac{f\,x_s}{k_B T}\right) \qquad (5)$$

Here, k_s and k_c are the dissociation rate constants for the slip (s) and the catch (c) dissociation pathway, x_s and x_c are the widths of the corresponding energy barriers and $k_B T$ is the thermal energy. Especially the catch bond characteristics of P-Selectin/PSGL-1 has been approximated reasonably well by this approach [36-38]. Of note, this model implies brittle bonds at zero load as the complex lifetime decreases for diminishing external forces.
However, there are host guest systems like hydrophilic domain (HD) of the human extracellular enzyme sulfatase-1 (Sulf1) and glycosaminoglycan heparansulfate (HS) that expose catch bond behavior in an intermediate force range (approx. 10 – 20 pN) and slip dissociation for vanishing external force (Fig.10a).

Correspondingly, a one state two path approach is not applicable to systems of this type as it diverges in the low force regime. More elaborate approaches have been reported that take account of force induced deformations [39], protein water interfaces [40], fluctuating energy barriers [41] or two bound states separated by an energy barrier [31, 35, 42-47] which we will present here:

By introducing a coupled, double-well energy landscape with two well confined binding states S_1 and S_2 separated by the energy barriers E_{12} and E_{21}, respectively (Fig.10b).

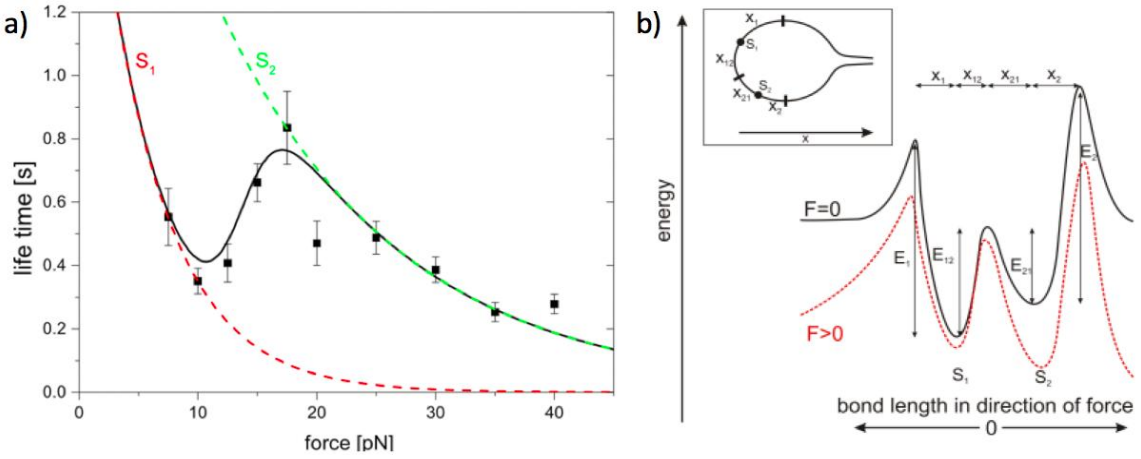

Fig. 10: *a) Experimental complex lifetimes for the HD substrate HS under a constant external force in the range of 7.5 – 40 pN (scatter plots). HS shows explicit catch bond behavior in the force range of 10 – 18 pN. The dashed red and green plots represent the slip dissociation from the individual binding states S_1 and S_2, respectively. b) Flat and 2D (inset) representation of the proposed energy landscape for HD/HS interaction. The occupancy of both bound states S_1 and S_2 is governed by equilibrium thermodynamics. In the force free state (black plot) solely S_1 is populated and dissociation can be observed from this state only. Upon applying a force the binding potential is tilted (red plot). In the intermediate force (transition) regime the system can flip between S_1 and S_2 by surpassing the internal energy barriers E_{12} and E_{21}, respectively. Consequently, the observed unbinding events are a superposition of both states. Increasing the force further depopulates S_1 successively and only dissociation from S_2 can be observed. Figures adapted with courtesy from [31].*

Both states individually obey slip bond characteristics and dissociation can occur from either of the two states depending on the external force. The total width of this barrier is given by $x = x_{12} + x_{21}$. The system can dissociate either from the low force state S_1via x_1 or from the high force state S_2via x_2 by crossing the corresponding barriers E_1 or E_2, respectively.

We can assume that both binding states can be attributed to different molecular conformations. Hence, it is reasonable to neglect higher order dissociation (e.g. S_1 via x_{12} and x_2) or dissociation from transition states when the conformational relaxation is fast compared to a single pulling experiment. As protein folding dynamics are in the range of micro to milliseconds [48-50] the upper temporal limit for HD conformational dynamics can be estimated to be in this range or even below. For comparison, the timescale of a molecular stretching experiment is in the range of seconds to tens of milliseconds.

Consequently, the population of the states S_1 and S_2 is in thermodynamic equilibrium at any time of the experiment and can therefore be calculated by equilibrium thermodynamics. To estimate the (force dependent) population of the two states we introduce the canonical partition function Z(f) as a function of the external force.

$$Z(f) = \exp\left(\frac{E_{12} - f\,x_{12}}{k_B T}\right) + \exp\left(\frac{E_{21} - f\,x_{21}}{k_B T}\right) \qquad (6)$$

With the energy difference $\Delta E = E_{12} - E_{21}$ and the compliance length $\Delta x = x_{12} - x_{21}$ of both states, we derive the population probability $p_1(f)$ and $p_2(f)$ of the states S_1 and S_2.

$$p_1(f) = \left(1 + \exp\left(-\frac{(\Delta E - f\,\Delta x)}{k_B T}\right)\right)^{-1} \quad (7)$$

$$p_2(f) = \left(1 + \exp\left(\frac{(\Delta E - f\,\Delta x)}{k_B T}\right)\right)^{-1} \quad (8)$$

In line with the afore-introduced Kramers-Bell-Evans (KBE) model for slip bonds ====[6-7] we define the total dissociation rate $k(f)$ as the probability weighted sum of the dissociation rates from S_1 and S_2.

$$k(f) = p_1(f) k_1 \exp\left(\frac{f x_1}{k_B T}\right) + p_2(f) k_2 \exp\left(\frac{f x_2}{k_B T}\right) \quad (9)$$

Here, the state from which the system dissociates explicitly depends on the applied force f, the shape of the binding potential landscape, parameterized by the compliance length Δx and the energy difference ΔE between S_1 and S_2.

Within this theoretical framework one explicitly observes three different dissociation regimes at low, medium and high forces: At low and high forces solely S_1 or S_2 is populated (Fig.10b Inset). Therefore, force clamp experiments within these force ranges show dissociation of slip type (Fig.3b dashed plots), thus yielding the corresponding dissociation rate constants (k_1, k_2) and bond lengths (x_1, x_2). In contrast, when performing force clamp experiments at intermediate forces, the HD/HS complex can dissociate either from S_1 **or** S_2. Hence, force clamp datasets obtained within this force regime comprise individual complex life times of both states and the average life time τ is therefore a superposition of S_1 and S_2.

Despite the small number of molecular systems exposing catch bond behavior there are several models describing the same. So far, there is a vital discussion about the interpretation of catch bond characteristics. Nevertheless, this exotic and unintuitive binding surely indicates a non-trivial energy landscape.

3 Summary and Outlook

The investigation of interactions between single molecules and the manipulation of structures on the molecular scale is an interdisciplinary task. Although commercial atomic force microscopes are readily available, exploiting the entire potential of these instruments requires detailed knowledge and experience. On the other hand, a general understanding of (bio-) chemical issues, the synthesis of tailor-made molecules and the preparation of specifically functionalized surfaces are just as important for successful experiments. But as diverse the requirements are, as multifaceted are the topics that can be addressed with this technique. The presented examples show that the binding in complexes with a wide range of affinities can be studied and dynamic processes as optomechanical switching can be followed.

There are a multitude of research areas that might get essential progress by the information accessible from single-molecule force spectroscopy experiments. Fundamental questions of theoretical physics might be addressed in studies on sophisticated biomolecular complexes and supramolecular structures. SMFS experiments on simple model complexes can help to develop mathematical models for macroscopic processes as adhesion, mechanical wear and (biological) recognition events. The impact of forces on interactions between the building blocks of (large) non-covalently linked aggregates, dynamic systems, chemical reactions and connections between surfaces mediated by supramolecular interactions is already under investigation. In the general view, single molecule force spectroscopy connects characteristic binding parameters of the macroscopic with the microscopic, molecular world.

References

[1] Fischer, E. *Berichte der deuschen chemischen Gesellschaft* (1894).
[2] Rief, M., Gautel, M., Oesterhelt, F.and Fernandez, J., and Gaub, H. *Science* **276**, 1109–1112 (1997).
[3] Dammer, U., Popescu, O., Wagner, P., Anselmetti, D., Güntherodt, H. J., and Misevic, G. N. *Science* **267**(5201), 1173–1175 (1995).
[4] Florin, E. L., Moy, V. T., and Gaub, H. E. *Science* **264**(5157), 415–417 (1994).
[5] Lee, G. U., Chrisey, L. A., and Colton, R. J. *Science* **266**(5186), 771–773 (1994).
[6] Evans, E. and Ritchie, K. *Biophys. J.* **72**(4), 1541–1555 Apr (1997).
[7] Bell, G. I. *Science* **200**(4342), 618–627 May (1978).
[8] Kramers, H. A. *Physica* **7**, 284–304 (1940).
[9] Smoluchowski, M. *Sitzungsberichte d. Kais. Ak. d. Wiss. in Wien. Math.-naturw. Klasse* (1915).
[10] Ritzefeld, M., Walhorn, V., Kleineberg, C., Bieker, A., Kock, K., Herrmann, C., Anselmetti, D., and Sewald, N. *Biochemistry* **52**(46), 8177–8186 Nov (2013).
[11] Wollschläger, K., Gaus, K., Körnig, A., Eckel, R., Wilking, S.-D., McIntosh, M., Majer, Z., Becker, A., Ros, R., Anselmetti, D., and Sewald, N. *Small* **5**(4), 484–495 Apr (2009).
[12] Lehn, J. M. *Science* **260**(5115), 1762–1763 Jun (1993).
[13] Lehn, J.-M. *Angewandte Chemie International Edition in English* **27**(1), 89–112 (1988).
[14] Nguyen, S. T., Gin, D. L., Hupp, J. T., and Zhang, X. *Proc Natl Acad Sci U S A* **98**(21), 11849–11850 Oct (2001).
[15] Anselmetti, D., Bartels, F. W., B., A., Decker, B., Eckel, R., McIntosh, M., Mattay, J., Plattner, P., Ros, R., Schafer, C., and Sewald, N. *Langmuir* **24**(4), 1365–1370 (2008). PMID: 18062710.
[16] Eckel, R., Ros, R., Decker, B., Mattay, J., and Anselmetti, D. *Angew. Chem. Int. Ed.* **44**(3), 484–488 (2005).
[17] Schäfer, C., Decker, B., Letzel, M., Novara, F., Eckel, R., Ros, R., Anselmetti, D., and Mattay, J. *Pure Appl. Chem.* **78**, 2247–2259 (2006).
[18] Schäfer, C., Eckel, R., Ros, R., Mattay, J., and Anselmetti, D. *J Am Chem Soc* **129**(6), 1488–1489 (2007).
[19] Dembo, M., Torney, D. C., Saxman, K., and Hammer, D. *Proceedings of the Royal Society of London. Series B: Biological Sciences* **234**(1274), 55–83 Jun (1988).
[20] Marshall, B. T., Long, M., Piper, J. W., Yago, T., McEver, R. P., and Zhu, C. *Nature* **423**(6936), 190–193 May (2003).
[21] Bartels, F. W., McIntosh, M., Fuhrmann, A., Metzendorf, C., Plattner, P., Sewald, N., Anselmetti, D., Ros, R., and Becker, A. *Biophys J* **92**(12), 4391–4400 Jun (2007).
[22] Dammer, U., Hegner, M., Anselmetti, D., Wagner, P., Dreier, M., Huber, W., and Güntherodt, H. J. *Biophys. J.* **70**(5), 2437–2441 May (1996).
[23] Eckel, R., Wilking, S. D., Becker, A., Sewald, N., Ros, R., and Anselmetti, D. *Angew. Chem. Int. Ed.* **44**(25), 3921–3924 (2005).
[24] Fuhrmann, A., Schoening, J. C., Anselmetti, D., Staiger, D., and Ros, R. *Biophys J* **96**(12), 5030–5039 Jun (2009).
[25] Harder, A., Walhorn, V., Dierks, T., Fernández-Busquets, X., and Anselmetti, D. *Biophys J* **99**(10), 3498–3504 Nov (2010).
[26] Hinterdorfer, P., Baumgartner, W., Gruber, H. J., Schilcher, K., and Schindler, H. *Proc. Nat. Acad. Sci. U S A* **93**(8), 3477–3481 Apr (1996).
[27] Moy, V. T., Florin, E. L., and Gaub, H. E. *Science* **266**(5183), 257–259 (1994).
[28] Schröder, T., Geisler, T., Walhorn, V., Schnatwinkel, B., Anselmetti, D., and Mattay, J. *Phys Chem Chem Phys* **12**(36), 10981–10987 Sep (2010).
[29] Walhorn, V., Schäfer, C., Schröder, T., Mattay, J., and Anselmetti, D. *Nanoscale* **3**(11), 4859–4865 Nov (2011).
[30] Guo, B. and Guilford, W. H. *Proceedings of the National Academy of Sciences* **103**(26), 9844–9849 (2006).

[31] Harder, A., Möller, A.-K., Milz, F., Neuhaus, P., Walhorn, V., Dierks, T., and Anselmetti, D. *submitted* (2015).
[32] Kong, F., García, A. J., Mould, A. P., Humphries, M. J., and Zhu, C. *J Cell Biol* **185**(7), 1275–1284 Jun (2009).
[33] Thomas, W. E., Trintchina, E., Forero, M., Vogel, V., and Sokurenko, E. V. *Cell* **109**(7), 913 – 923 (2002).
[34] Yago, T., Lou, J., Wu, T., Yang, J., Miner, J. J., Coburn, L., López, J. A., Cruz, M. A., Dong, J.-F., McIntire, L. V., McEver, R. P., and Zhu, C. *J Clin Invest* **118**(9), 3195–3207 Sep (2008).
[35] Bartolo, D., Derényi, I., and Ajdari, A. *Phys Rev E Stat Nonlin Soft Matter Phys* **65**(5 Pt 1), 051910 May (2002).
[36] Evans, E., Leung, A., Heinrich, V., and Zhu, C. *Proc Natl Acad Sci U S A* **101**(31), 11281–11286 Aug (2004).
[37] Pereverzev, Y. V., Prezhdo, O. V., Forero, M., Sokurenko, E. V., and Thomas, W. E. *Biophys J* **89**(3), 1446–1454 Sep (2005).
[38] Cheung, L. S.-L., Raman, P. S., Balzer, E. M., Wirtz, D., and Konstantopoulos, K. *Phys Biol* **8**(1), 015013 Feb (2011).
[39] Pereverzev, Y. V. and Prezhdo, O. V. *Phys. Rev. E* **73**, 050902 May (2006).
[40] Pereverzev, Y. V., Prezhdo, O. V., and Sokurenko, E. V. *The Journal of Physical Chemistry B* **112**(36), 11440–11445 (2008). PMID: 18710275.
[41] Liu, F. and Ou-Yang, Z.-c. *Phys. Rev. E* **74**, 051904 Nov (2006).
[42] Barsegov, V. and Thirumalai, D. *Proc Natl Acad Sci U S A* **102**(6), 1835–1839 Feb (2005).
[43] Barsegov, V. and Thirumalai, D. *The Journal of Physical Chemistry B* **110**(51), 26403–26412 (2006). PMID: 17181300.
[44] Beste, M. T. and Hammer, D. A. *Proc Natl Acad Sci U S A* **105**(52), 20716–20721 Dec (2008).
[45] Pereverzev, Y. V., Prezhdo, E., and Sokurenko, E. V. *Biophys J* **101**(8), 2026–2036 Oct (2011).
[46] Suzuki, Y. and Dudko, O. K. *Phys. Rev. Lett.* **104**, 048101 Jan (2010).
[47] Thomas, W., Forero, M., Yakovenko, O., Nilsson, L., Vicini, P., Sokurenko, E., and Vogel, V. *Biophys J* **90**(3), 753–764 Feb (2006).
[48] Klepeis, J. L., Lindorff-Larsen, K., Dror, R. O., and Shaw, D. E. *Current Opinion in Structural Biology* **19**(2), 120 – 127 (2009). Theory and simulation / Macromolecular assemblages.
[49] Lee, T.-H., Gonzalez, J. I., and Dickson, R. M. *Proc. Natl. Acad. Sci.* **99**(16), 10272–10275 Aug (2002).
[50] Yang, W. Y. and Gruebele, M. *Nature* **423**(6936), 193–197 May (2003).